The effect of annealing temperature and time on synthesis of graphene thin films by rapid thermal annealing

Jovana Prekodravac[a], Zoran Marković[a], Svetlana Jovanović[a], Milica Budimir[a], Davor Peruško[a], Ivanka Holclajtner-Antunović[b], Vladimir Pavlović[c], Zois Syrgiannis[d], Aurelio Bonasera[e] and Biljana Todorović-Marković[a]

[a]Vinča Institute of Nuclear Sciences, University of Belgrade, Mike Alasa 12-14, 11001 Belgrade, Serbia

[b]Faculty of Physical Chemistry, University of Belgrade, Studentski trg 12-16, 11158 Belgrade, Serbia

[c]Joint Laboratory for Advanced Materials, Serbian Academy of Sciences and Arts, 11000 Belgrade, Serbia

[d]Dipartimento di Scienze Farmaceutiche, Università degli Studi di Trieste, P.le Europa 1, 34127 Trieste, Italia

[e]Humboldt-Universität zu Berlin, Institut für Chemie, Brook-Taylor-Straße 2, D-12489 Berlin

*corresponding author at: Vinča Institute of Nuclear Sciences, University of Belgrade, Mike Alasa 12-14, 11001 Belgrade, Serbia

E-mail address: prekodravac@vinca.rs (Jovana Prekodravac)

Abstract

In this paper, we performed synthesis of graphene thin films by rapid thermal annealing (RTA) of thin nickel-copper (Ni/Cu) layers deposited on spectroscopic graphite as a carbon source. Furthermore, we investigated the effect of annealing temperature and annealing time on formation and quality of synthesized graphene

films. Raman spectroscopy study showed that annealing at lower temperatures results in formation of monolayer graphene films, while annealing at higher temperatures results in formation of multilayer graphene films. We used Raman mapping to determine the distribution of graphene sheets. Surface morphology of graphene thin films was investigated by atomic force microscopy and scanning electron microscopy with EDS probe.

Graphical abstract

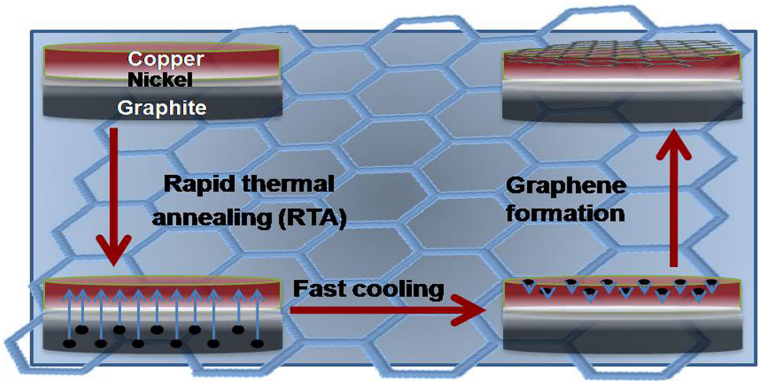

Highlights

- Graphene thin films were synthesized by RTA method
- Spectroscopic graphite was used as a carbon source for graphene synthesis
- Number of graphene layers increases with the increase of annealing temperatures
- Quality of graphene thin films increases with prolongation of annealing time

Keywords

Thin films, graphite, graphene, rapid thermal annealing

1. Introduction

Graphene is a single-atom-thick sheet with sp^2 hybridized carbon network hexagonally arrayed [1]. Recently graphene was described as the thinnest material in our universe [2]. Graphene is transparent, extremely strong and rigid material with high elasticity and surface area, high charge carrier mobility at room temperature and high thermal conductivity [3-6]. Due to structural, electrical, mechanical and chemical properties, graphene has attracted remarkable attention by research community [7-12]. These properties enable the usage of this material for nanoelectronic applications, bioelectronic, gas sensors, hydrogen storage devices, lithium batteries and supercapacitors [13-19].

Novoselov and co-workers [9] produced graphene for the first time in 2004, from graphite by mechanical exfoliation. Since then, graphene has been synthesized in many different ways. There are several primary synthesis methods for producing graphene, however all of these methods come with drawbacks as well. The drawbacks are mainly related to the time required for the synthesis and price of used method, or quality of obtained graphene films. Today, the most used methods are chemical vapor deposition (CVD), the epitaxial growth on silicon carbide, liquid exfoliation of graphite crystals, chemical reduction of graphene oxide and rapid thermal annealing (RTA) [20-28].

In this paper, we present graphene synthesis by RTA method in vacuum from thin Ni/Cu layers deposited on polished polycrystalline spectroscopic graphite as a carbon source. The samples were annealed at different annealing temperatures and with different annealing times in order to investigate the effect of annealing temperatures and annealing time on formation and quality of monolayer and multi-layer graphene films.

2. Materials and methods

2.1. Sample preparation

Samples were prepared by cutting the graphite spectroscopic electrodes (99.999% purity, Ringsdorff Spektralkohlestäbe, höchster Reinheit, SGL Carbon, Germany) into small pieces with diameter of 12.5 mm. Sample surface was polished with diamond pastes. Ni/Cu metal films were then deposited on graphite substrates in a single vacuum run, without heating of the graphite substrates. The deposition was carried out by direct-current (DC) sputtering (Balzers Sputtron II system, Switzerland) using 1.3 keV argon (Ar) ions and 99.9 % pure Ni and Cu targets. The base pressure in chamber was $7x10^{-6}$ mbar and the Ar partial pressure during deposition was $1x10^{-3}$ mbar. The first deposited thin metal layer was Ni with deposition rate of 9.5 nm/min and the second one was Cu with deposition rate of 16 nm/min. Thickness of individual thin Ni and Cu films, measured by profilometry, were 50 nm for Ni and 700 nm for Cu [29].

The samples were annealed in a vacuum furnace (TorVac system, United Kingdom), at different annealing temperatures, at 600 °C, 700 °C, 800 °C and 900 °C for 30 min followed by rapid cooling. Another set of samples was annealed at 900 °C for different annealing times: 30 min, 2h and 3h.

2.2. Sample characterization

Raman spectra of as-deposited and annealed samples were obtained by DXR Raman microscope (Thermo Scientific) using a 532 nm laser as excitation source. The laser power was kept at 2 mW to avoid heating of the sample with a pixel-to-pixel spectral resolution of 1 cm^{-1}.

The distribution of graphene sheets was obtained by Raman mapping with Renishaw inVia 15 Reflex, equipped with three laser sources and directly interfaced to a confocal microscope Leika DM-LM. The excitation radiation was generated by a Nd:YAG laser (532 nm), He-Ne laser (632.8 nm) and a Ti: sapphire laser (785 nm). The scanned area of the sample was 15 x 25 μm^2.

Surface morphology of as-deposited and annealed Ni/Cu thin films was analyzed with atomic force microscopy (AFM). AFM measurements were performed using Quesant microscope (Ambios Technology, USA) operating in tapping mode in air at room temperature. All images were obtained at 1 Hz, with 512 x 512 pixels image definition over different square areas. The average size of objects in AFM images and root mean square roughness (RMS) were determined by Gwyddion software [30].

The morphology of the films was characterized by scanning electron microscopy (SEM, JEOL JSM-6390LV) in vacuum at room temperature, with 15 kV acceleration voltage. Samples elementary composition was obtained with Energy Dispersive Spectroscopy (EDS, Oxford Aztec X-max). The scanned surface area was 1 x 1 mm^2.

3. Results and discussion

3.1. Raman Spectroscopy

Raman spectroscopy is very important tool for the study of different allotropes of carbon, since it is very sensitive to geometric structure and bonding within molecules. The Raman spectra of graphene show two main bands designed as the G and 2D bands. The third, D band may also be apparent in graphene Raman spectra if there are defects present in carbon lattice [31]. The G band is sharp and

appears at around 1587 cm^{-1}. The existence of G band corresponds to the in-plane vibration mode involving the sp^2 hybridized carbon atoms that comprise the graphene sheet. With the G band position, one can determine the number of layers present in the sample. However, the G band position can be affected by temperature and doping thus, intensity of the G band is more accurate way to determine graphene thickness. The D band is disorder or the defect band that appears at around 1350 cm^{-1} and it has been attributed to in-plane A_{1g} zone edge mode. The intensity of the D band can indicate the quality of graphene. By specifying intensity ratio of D and G bands (I_D/I_G) it is possible to define the level of defects present in the sample [31]. The 2D band is sharp, appears at around 2680 cm^{-1}, and it is the result of a two phonon lattice vibration process. Therefore intensity of 2D band can be used to determine graphene layer thickness based on the 2D and G bands intensity ratio (I_{2D}/I_G) [32-33]. If the intensity ratio of these bands is two or higher, single layer graphene is present in the sample.

In **Fig. 1** we present Raman spectra of Ni/Cu thin films annealed at different annealing temperatures for 30 min. In Raman spectra of the samples annealed at 600 °C and 700 °C, sharp 2D band at ~2700 cm^{-1} is more intense than the G band. Based on 2D-to-G intensity ratio (I_{2D}/I_G), ~3.57 and ~1.72 respectively (**Table 1.**), it was suggested the formation of monolayer graphene films in these samples. By fitting these 2D bands with one Lorentzian it was confirmed the formation of single layer graphene. Full width at half maximum (FWHM) was ~26 cm^{-1} for samples annealed at 600 °C, and ~37 cm^{-1} for samples annealed at 700 °C, which is characteristic for the single layer graphene [34].

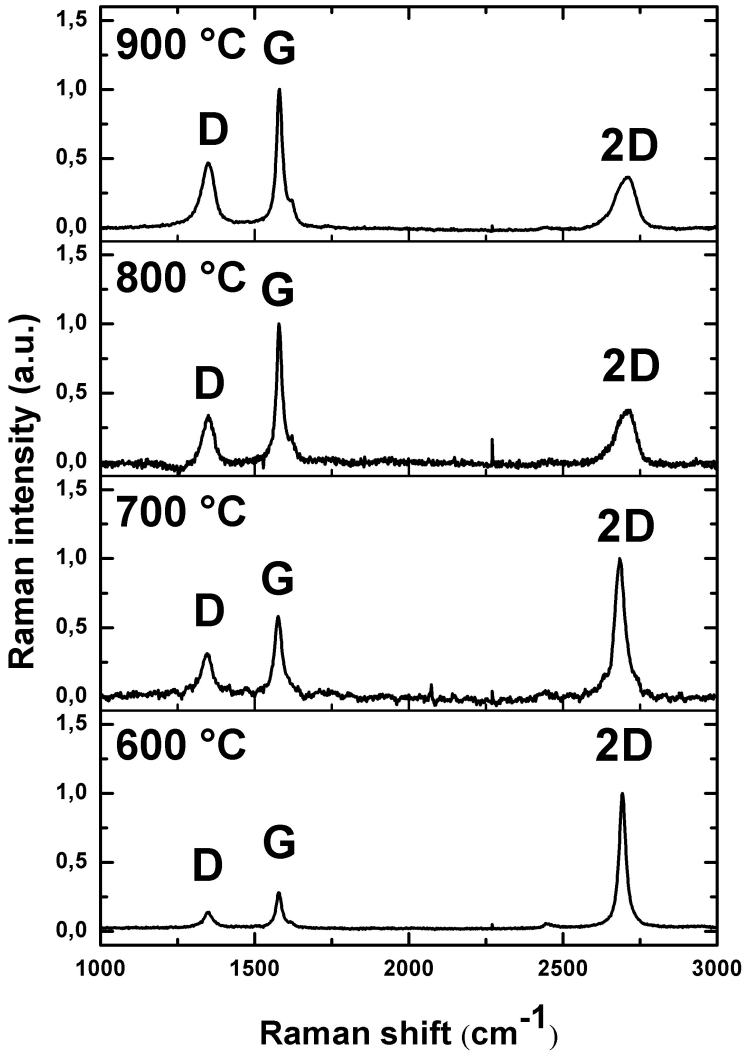

Fig. 1

Raman spectra of Ni/Cu thin films annealed at 600 °C, 700 °C, 800 °C and 900 °C in vacuum for 30 min.

Raman spectra of samples annealed at 800 °C and 900 °C showed some changes in 2D band shape and intensity. Here, intensity of the G band is much higher than intensity of the 2D band, while its shape is less symmetric which is characteristic for multilayer graphene. The presence of multilayer graphene was also confirmed with 2D-to-G intensity ratio (I_{2D}/I_G) presented in **Table 1**, where I_{2D}/I_G intensity ratio for the samples annealed at 800 °C was ~0.64, while in samples

annealed at 900 °C it amounts ~0.36. FWHM values for samples annealed at 800 °C were ~71 cm^{-1}, and ~77 cm^{-1} for samples annealed at 900 °C which is characteristic for multilayer graphene [34].

Table 1.

The D-to-G intensity ratio (I_D/I_G), 2D-to-G intensity ratio (I_{2D}/I_G) and the FWHM values of the samples annealed at different temperatures for 30 min.

Sample annealed for 30 min	**I_D/I_G**	**I_{2D}/I_G**	**FWHM (cm^{-1})**
600 °C	0.50	3.57	26
700 °C	0.53	1.72	37
800 °C	0.34	0.46	71
900 °C	0.47	0.36	77

From I_{2D}/I_G intensity ratio in **Table 1,** it was confirmed that annealing at 600 °C and 700 °C leads to the formation of single layer graphene films, while annealing at 800 °C and 900 °C results in formation of multilayer graphene films. Here, it can also be seen a higher level of defects (I_D/I_G) in samples annealed at lower annealing temperatures comparing to the samples that were annealed at higher annealing temperatures. Level of defects decreases with the increase of annealing temperature.

Since annealing at higher temperatures results in smaller defect level, another set of samples were annealed at 900 °C for different annealing times. **Fig. 2** presents Raman spectra of the samples annealed at 900 °C for 30 min, 2h and 3h.

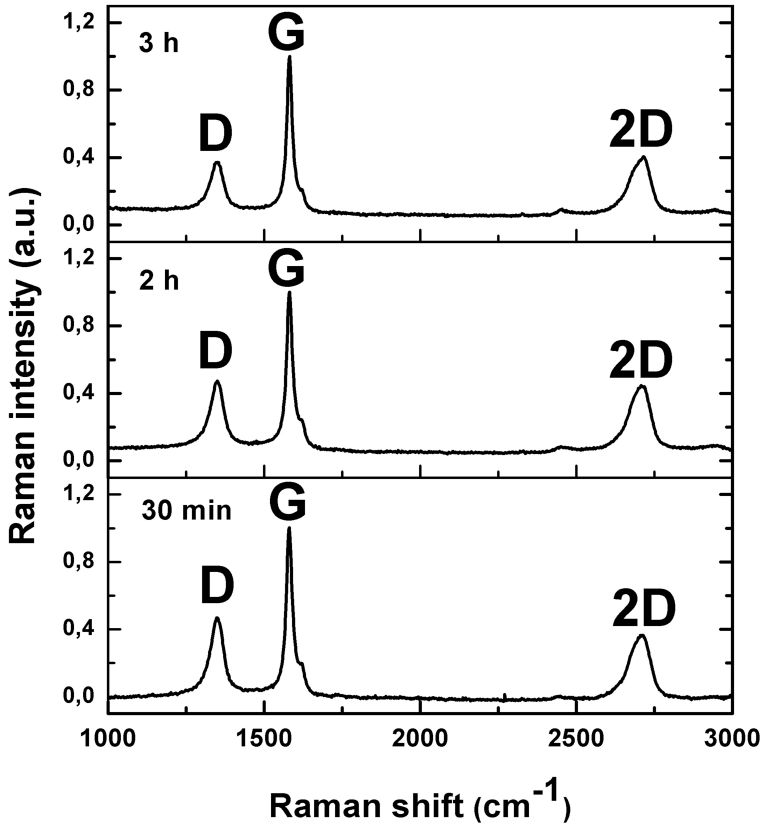

Fig. 2

Raman spectra of the samples annealed at 900 °C for 30 min, 2h and 3h.

Results presented in **Fig. 2** show that intensity of the G band is much higher than the intensity of the 2D band, while 2D band shape is not symmetric. The 2D-to-G intensity ratio (I_{2D}/I_G) for these samples, going from 30 min to 3h of annealing time, were ~0.36, ~0.45 and ~0.40, while FWHM values were ~77 cm^{-1}, ~71 cm^{-1} and ~72 cm^{-1} respectively (**Table 2**). These values of I_{2D}/I_G and FWHM are characteristic for multilayer graphene films [34]. Based on the results from **Fig. 2,** it can be concluded that annealing of the samples at 900 °C for different annealing times leads to the formation of homogenous multilayer graphene films. Prolongation of annealing time affects the level of defects presented in the samples. By calculating the D-to-G intensity ratio (I_D/I_G) (**Table 2**), it can be seen that the level of defects decreases with

prolongation of annealing time. The D-to-G intensity ratio (I_D/I_G), 2D-to-G intensity ratio (I_{2D}/I_G) and the FWHM values of the samples annealed at 900 °C for 30 min, 2h and 3h are given in **Table 2**.

Table 2.

The D-to-G intensity ratio (I_D/I_G), 2D-to-G intensity ratio (I_{2D}/I_G) and the FWHM values of the samples annealed in samples annealed at 900 °C for 30 min, 2h and 3h.

Samples annealed at 900 °C	**I_D/I_G**	**I_{2D}/I_G**	**FWHM (cm^{-1})**
30 min	0.47	0.36	77
2h	0.46	0.45	71
3h	0.37	0.40	72

3.2. Raman mapping

Raman microscopy was used for quite a long time to generate chemical maps. This non-destructive technique is particularly well suited to analyze and display the distribution of various chemical compounds within a sample down to the submicron level. Raman mapping entails the coordinated measurement of Raman spectra with successive movements of the sample by a specified distance. Numerous types of samples qualify for such analysis so as carbon materials, i.e. graphene. These way graphene samples may be characterized in regards to whether the sample is composed entirely of one layer across the whole sample or it contains areas with different thicknesses. In **Fig. 3** we present 3D Raman mapping image of the sample annealed at 900 °C for 3h. The optical view of the scanned area (15 x 25 μm^2) of the sample is presented in the inset of **Fig. 3**, where the total number of recorded spectra was 70. The 3D Raman mapping image of graphene shows three main

bands designed as the D band (~1350 cm^{-1}), G band (~1587cm^{-1}) and 2D band (~2680 cm^{-1}). Here it can be seen that the sample surface is composed entirely of multi layer graphene which is evident from the much higher G band intensity compared to the intensity of 2D band. To determine the values of 2D-to-G bands (I_{2D}/I_G) and D-to-G bands (I_D/I_G) intensity ratios from **Fig. 3** we randomly selected 35 spectra of 70 recorded. These values were determined to be 0.34 ± 0.07 for 2D-to-G and 0.57 ± 0.03 for D-to-G intensity ratio. Based on these results it was confirmed the formation of homogenous multilayer graphene films across the sample surface with a relatively high level of defects.

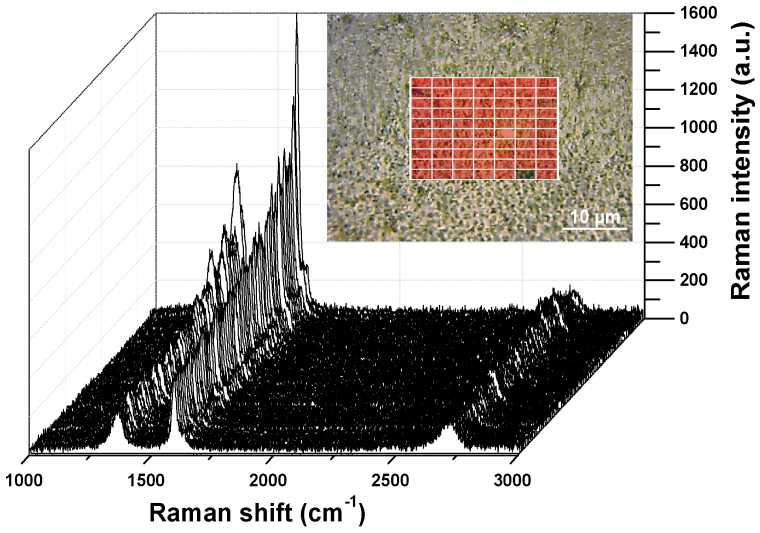

Fig. 3

3D Raman mapping image of the sample annealed at 900 °C for 3h. In the inset, the optical view of the scanned area (15 x 25 μm^2) of the sample was shown.

3.3. AFM analysis

Atomic force microscopy (AFM) was used to visualize surface morphology of as-deposited and annealed thin films. **Fig. 4** presents 3D view AFM surface morphology images of Ni/Cu thin films annealed for 30 min at different temperatures. The range

of the displayed data and the color bar in micrometers (μm) are shown on the right side of the AFM images. Presented results show the formation of Ni/Cu alloy, during annealing in vacuum. The Ni/Cu alloy has granular morphology [35] about 2 μm in size. Thus, from AFM images it was not possible to observe the formation of graphene thin films. RMS roughness of the samples, determined by Gwyddion software was approximately 200 nm for the samples annealed at 600 °C, 700 °C and 800 °C. This high RMS values origin from Ni/Cu alloy. Sample annealed at 900 °C, however showed RMS roughness about 166 nm. It is the result of higher solubility of carbon atoms in Ni at higher temperatures (Table 3), which enables uniform diffusion of carbon atoms through Ni/Cu grain boundaries to the top of the sample. Therefore, there is the formation of thicker, more homogenous layer of multilayer graphene films at the sample surface that covers the Ni/Cu granular alloy.

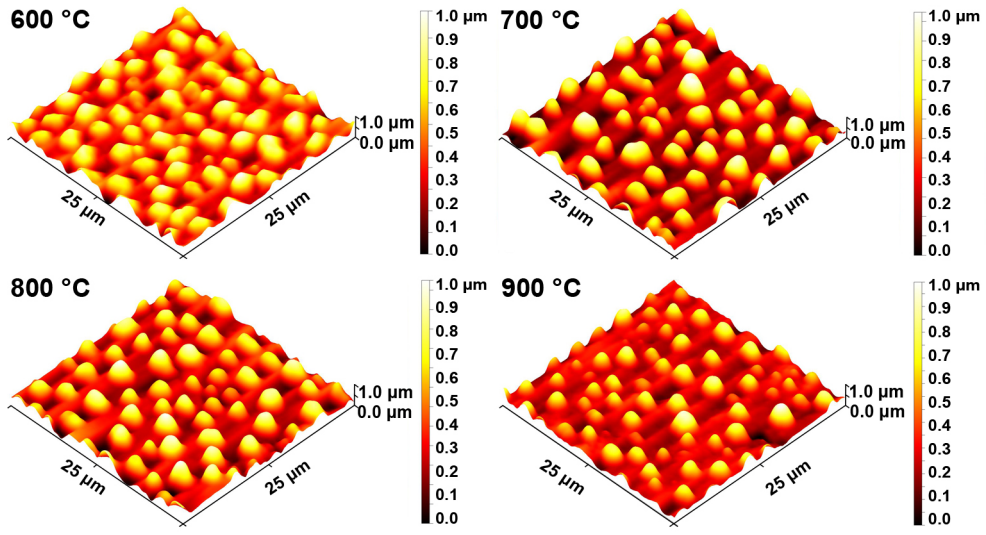

Fig. 4

3D view AFM surface morphology images of Ni/Cu thin films annealed in vacuum for 30 min at 600 °C, 700 °C, 800 °C and 900 °C.

Surface morphology images of as-deposited Ni/Cu thin films and Ni/Cu thin films annealed at 900 °C for different annealing times are presented in **Fig. 5**. Here it can be seen that granular morphology of Ni/Cu alloy appears in the sample annealed for 30 min, while samples annealed for 2h and 3h did not show granular surface. The RMS roughness of the sample before annealing was 19.4 nm, while after annealing at 900 °C for different annealing times there was significant change in RMS roughness. After annealing for 30 min, the RMS roughness increased to 166 nm because of the Ni/Cu alloy formation. With prolongation of annealing time, the RMS roughness of the samples decreased to 44 nm after annealing for 2h, and 13.9 nm after annealing for 3h. The formation of thicker, more homogenous layer of multilayer graphene films at the sample surface that covers the Ni/Cu granular alloy increases with prolongation of annealing time at 900 ºC causing a decrease in RMS values.

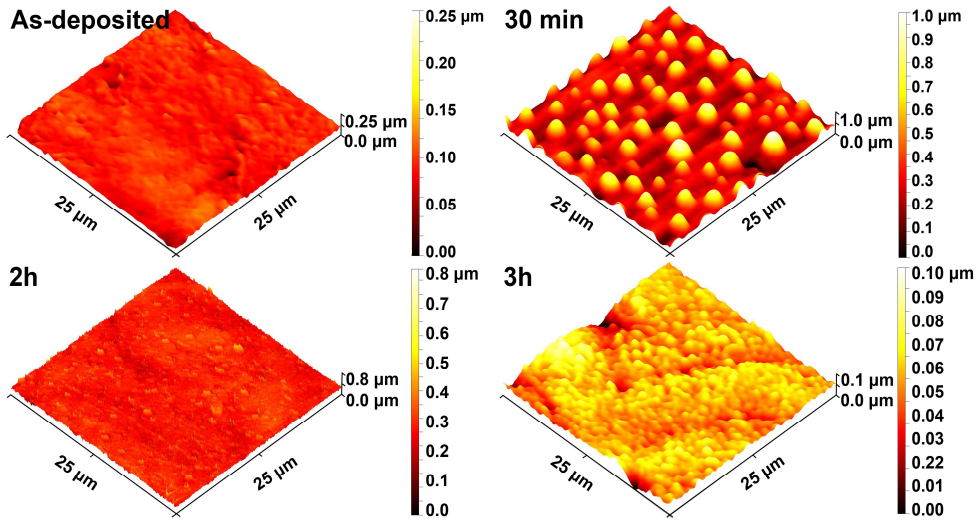

Fig. 5

3D view AFM surface morphology images of as-deposited Ni/Cu thin films and Ni/Cu thin films annealed in vacuum at 900 °C for 30 min, 2h and 3h.

3.4. SEM with EDS probe

Graphene layers especially if deposited on solid bulk substrate can be imaged and analyzed using SEM microscopy. The use of SEM also facilitates imaging and EDS analysis of graphene layers with respect to the substrate. **Fig. 6** shows SEM images of the sample annealed at 600 °C for 30 min. **Fig. 6a** presents the scanned area of the sample with granular morphology, which originates from Ni/Cu alloy [36]. Elementary analysis of the sample-scanned area (**Fig. 6b**) confirmed that the most abundant elements on the sample surface are carbon with 90 %, Cu with approximately 10 % and Ni in a low percent. **Figs. 6c-e** present distribution and relative proportion of defined elements. Red particles originate from carbon, green particles determine distribution of Cu while blue particles originates from Ni. Based on the literature data, that indicates the possible interaction of Ni and Cu at low temperatures, we concluded that there has been a formation of the Ni/Cu alloy in our sample after annealing at 600 ºC [35]. With AFM analysis, we confirmed this conclusion. Therefore, because of the strong Ni/Cu interaction the Ni elemental mapping presented in **Fig. 6e** shows great similarity to the Cu elemental mapping presented in **Fig. 6d**. However, the weight percent of the Ni (**Fig. 6b**) is in fact very small, approximately 2 %. Based on the results it was concluded that the formed graphene thin film was not homogenous.

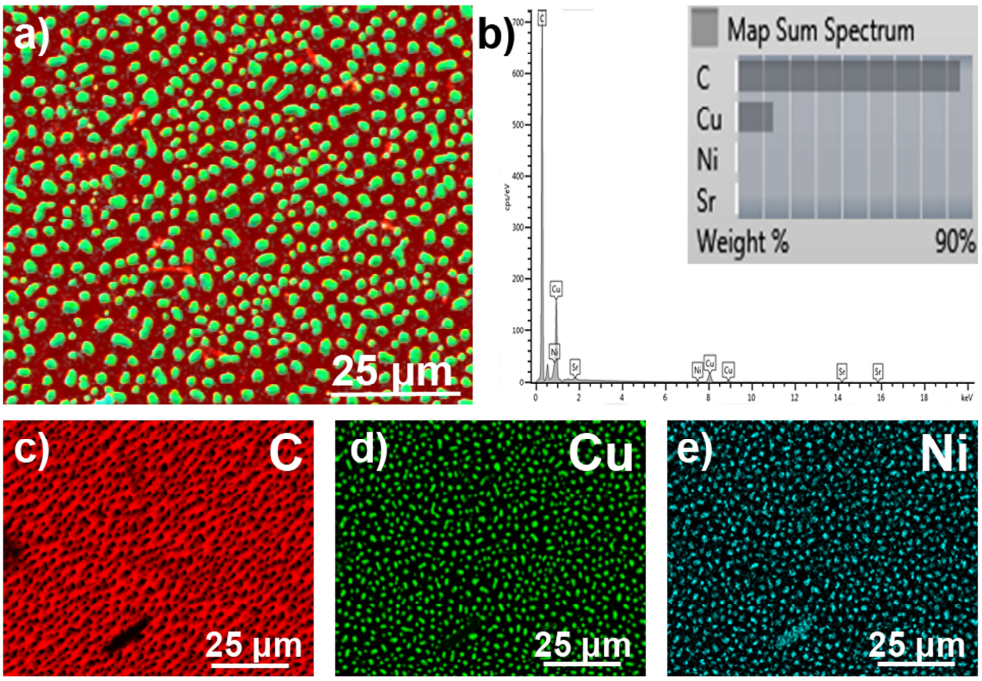

Fig. 6

EDS characterization of sample annealed at 600 °C for 30 min: (a) SEM image of the sample, (b) elemental composition for the region captured in (a), (c-e) distribution of defined elements over the scanned area of the sample.

Fig.7 presents SEM images of samples annealed at 900 °C for 3h. Here one can see that the samples surface area is 100 % coated with carbon, with low Ni percent (**Fig. 7b**). This means that there is no Ni/Cu alloy present on the sample surface, which was confirmed by the absence of granular morphology (**Fig 7a**). From **Figs. 7c,d** one can see the distribution of defined elements over the scanned area, where red particles originate from carbon and green particles correspond to the distribution of Ni. **Fig. 7e** presents the formation of multilayer graphene islands on the sample surface with approximately 190 µm in size.

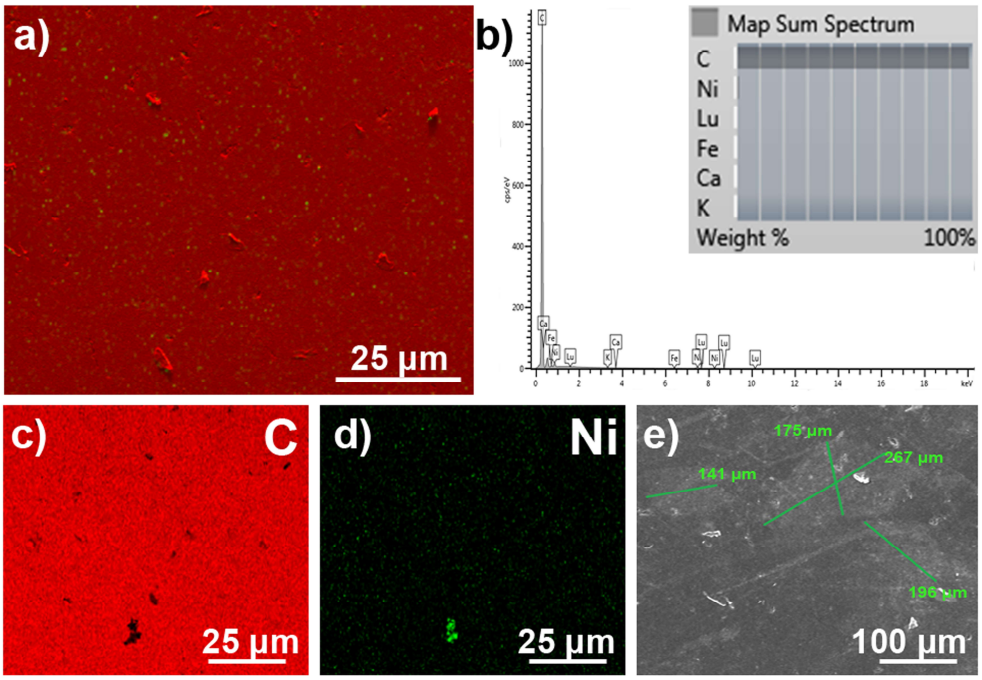

Fig. 7

EDS characterization of the sample annealed at 900 °C for 3h: (a) SEM image of the sample, (b) elemental composition for the region captured in (a), (c,d) distribution of defined elements over the scanned area of the sample, (e) formed graphene island on the sample surface.

4. Growing mechanism

Graphene formation with RTA method implies two main steps, annealing in vacuum, i.e. dissolving of carbon atoms in metals, and the fast cooling with crystallization of carbon atoms onto the metal surface to form graphene. The first deposited layer on graphite substrate was Ni because carbon atoms have extremely high solubility in Ni at elevated temperature which is very important for the first step of graphene synthesis. This allows carbon atom to diffuse through Ni/Cu grain boundaries to the top of the sample surface. The second deposited layer was Cu, wherein carbon atoms have low solubility, critical for the second synthetic step. Here,

during fast cooling carbon atoms do not have enough time to diffuse back into the bulk [37].

Graphene growth has been previously demonstrated on a variety of transitions metals [38-45]. Cu is specific between potential used metals because carbon exhibit a very low solubility in this metal, in addition the diffusion barrier of carbon atoms on Cu is very low. Cu surface acts as a self-limiting catalyst for graphene growth [37, 46]. Ni on the other hand, shows significant carbon solubility and high carbon diffusivity at higher temperatures, which decreases with a reduction of temperature [46]. The solubility of carbon in Ni, measured by parts per million atoms per cubic centimeter (ppma/cm^3), can be calculated based on an expression:

$$S_P = S_{PO}\, exp(H_P / kT) \quad (1)$$

where: S_{PO} is an entropic pre-factor related to density of sites where solute atoms sit; H_P is the heat of precipitation and k is Boltzmann's constant [47]. Solubility's of carbon in Ni versus annealing temperature are presented in **Table 3**.

Table 3. Solubility of carbon in Ni versus annealing temperature

Annealing temperature (°C)	Carbon solubility in nickel (ppma per cm^3)
600	2.4x10^{13}
700	4.1x10^{13}
800	6.3x10^{13}
900	9.2x10^{13}

Baraton et al. [47] defined temperature range in which for a given carbon concentration equilibrium thermodynamics would deliver monolayer graphene on

conveniently oriented nickel surfaces. Comparing their results to the results obtained in this work we concluded that monolayer graphene thin films would form only during annealing at 600 and 700 °C.

5. Conclusions

In this paper, we investigated the effect of annealing temperature and annealing time on formation and quality of graphene thin films. Our results suggest that annealing at lower annealing temperatures (600 ºC and 700 ºC) results in formation of single layer graphene thin films. These graphene thin films are not continuous and have relatively high level of defects. The annealing at higher annealing temperatures leads to formation of homogenous multilayer graphene thin films with lower defect level. We also confirmed that the defect level decreases with prolongation of annealing time.

Acknowledgements

This research was supported by the Ministry of Education, Science and Technological Development of Republic of Serbia (project no. 172003).

References

[1] A.K. Geim, K.S. Novoselov, The rise of graphene, Nat Mater, 6 (2007) 183-191.
[2] A.K. Geim, A.H. MacDonald, Graphene: Exploring carbon flatland, Phys Today, 60 (2007) 35-41.
[3] A.A. Balandin, S. Ghosh, W. Bao, I. Calizo, D. Teweldebrhan, F. Miao, C.N. Lau, Superior thermal conductivity of single-layer graphene, Nano Lett, 8 (2008) 902-907.
[4] K.I. Bolotin, K.J. Sikes, Z. Jiang, M. Klima, G. Fudenberg, J. Hone, P. Kim, H.L. Stormer, Ultrahigh electron mobility in suspended graphene, Solid State Commun, 146 (2008) 351-355.
[5] R.S. Edwards, K.S. Coleman, Graphene synthesis: relationship to applications, Nanoscale, 5 (2013) 38-51.
[6] R.R. Nair, P. Blake, A.N. Grigorenko, K.S. Novoselov, T.J. Booth, T. Stauber, N.M.R. Peres, A.K. Geim, Fine structure constant defines visual transparency of graphene, Science, 320 (2008) 1308-1308.
[7] A.H. Castro Neto, F. Guinea, N.M.R. Peres, K.S. Novoselov, A.K. Geim, The electronic properties of graphene, Rev Mod Phys, 81 (2009) 109-162.
[8] M.I. Katsnelson, K.S. Novoselov, A.K. Geim, Chiral tunnelling and the Klein paradox in graphene, Nat Phys, 2 (2006) 620-625.
[9] K.S. Novoselov, A.K. Geim, S.V. Morozov, D. Jiang, Y. Zhang, S.V. Dubonos, I.V. Grigorieva, A.A. Firsov, Electric field effect in atomically thin carbon films, Science, 306 (2004) 666-669.
[10] K.S. Novoselov, Z. Jiang, Y. Zhang, S.V. Morozov, H.L. Stormer, U. Zeitler, J.C. Maan, G.S. Boebinger, P. Kim, A.K. Geim, Room-temperature quantum hall effect in graphene, Science, 315 (2007) 1379-1379.
[11] Y.B. Zhang, Y.W. Tan, H.L. Stormer, P. Kim, Experimental observation of the quantum Hall effect and Berry's phase in graphene, Nature, 438 (2005) 201-204.
[12] C. Reiner-Rozman, M. Larisika, C. Nowak, W. Knoll, Graphene-based liquid-gated field effect transistor for biosensing: Theory and experiments, Biosens Bioelectron, 70 (2015) 21-27.
[13] B. Lobato, V. Vretenar, P. Kotrusz, M. Hulman, T.A. Centeno, Reduced graphite oxide in supercapacitor electrodes, J Colloid Interface Sci, 446 (2015) 203-207.
[14] S. Ghosh, I. Calizo, D. Teweldebrhan, E.P. Pokatilov, D.L. Nika, A.A. Balandin, W. Bao, F. Miao, C.N. Lau, Extremely high thermal conductivity of graphene: Prospects for thermal management applications in nanoelectronic circuits, Appl Phys Lett, 92 (2008) 1-3.
[15] L.H. Hess, M. Jansen, V. Maybeck, M.V. Hauf, M. Seifert, M. Stutzmann, I.D. Sharp, A. Offenhausser, J.A. Garrido, Graphene Transistor Arrays for Recording Action Potentials from Electrogenic Cells, Adv Mater, 23 (2011) 5045-5049.
[16] M. Pumera, Graphene-based nanomaterials for energy storage, Energ Environ Sci, 4 (2011) 668-674.
[17] F. Schedin, A.K. Geim, S.V. Morozov, E.W. Hill, P. Blake, M.I. Katsnelson, K.S. Novoselov, Detection of individual gas molecules adsorbed on graphene, Nat Mater, 6 (2007) 652-655.
[18] Y. Wang, J. Zhu, One-step electroplating porous graphene oxide electrodes of supercapacitors for ultrahigh capacitance and energy density, Nanotechnology, 26 (2015) 055401.
[19] S. Kumar, S. Kaushik, R. Pratap, S. Raghavan, Graphene on paper: a simple, low-cost chemical sensing platform, ACS Appl Mater Interfaces, 7 (2015) 2189-2194.
[20] C.K. Chua, M. Pumera, Chemical reduction of graphene oxide: a synthetic chemistry viewpoint, Chem Soc Rev, 43 (2014) 291-312.
[21] Y. Hernandez, V. Nicolosi, M. Lotya, F.M. Blighe, Z.Y. Sun, S. De, I.T. McGovern, B. Holland, M. Byrne, Y.K. Gun'ko, J.J. Boland, P. Niraj, G. Duesberg, S. Krishnamurthy, R. Goodhue, J. Hutchison, V. Scardaci, A.C. Ferrari, J.N. Coleman, High-yield production of graphene by liquid-phase exfoliation of graphite, Nat Nanotechnol, 3 (2008) 563-568.
[22] A. Reina, X.T. Jia, J. Ho, D. Nezich, H.B. Son, V. Bulovic, M.S. Dresselhaus, J. Kong, Layer Area, Few-Layer Graphene Films on Arbitrary Substrates by Chemical Vapor Deposition, Nano Lett, 9 (2009) 3087-3087.

[23] C. Riedl, C. Coletti, U. Starke, Structural and electronic properties of epitaxial graphene on SiC(0 0 0 1): a review of growth, characterization, transfer doping and hydrogen intercalation, J Phys D Appl Phys, 43 (2010) 1-27.
[24] W. Xiong, Y.S. Zhou, L.J. Jiang, A. Sarkar, M. Mahjouri-Samani, Z.Q. Xie, Y. Gao, N.J. Ianno, L. Jiang, Y.F. Lu, Single-Step Formation of Graphene on Dielectric Surfaces, Adv Mater, 25 (2013) 630-634.
[25] A.J. Strudwick, N.E. Weber, M.G. Schwab, M. Kettner, R.T. Weitz, J.R. Wunsch, K. Mullen, H. Sachdev, Chemical vapor deposition of high quality graphene films from carbon dioxide atmospheres, Acs Nano, 9 (2015) 31-42.
[26] W. Norimatsu, M. Kusunoki, Epitaxial graphene on SiC{0001}: advances and perspectives, Phys Chem Chem Phys, 16 (2014) 3501-3511.
[27] G. Shi, A. Michelmore, J. Jin, L.H. Li, Y. Chen, L.Z. Wang, H. Yu, G. Wallace, S. Gambhir, S.M. Zhu, P. Hojati-Talemi, J. Ma, Advancement in liquid exfoliation of graphite through simultaneously oxidizing and ultrasonicating, J Mater Chem A, 2 (2014) 20382-20392.
[28] J.H. Chu, J. Kwak, T.Y. Kwon, S.D. Park, H. Go, S.Y. Kim, K. Park, S. Kang, S.Y. Kwon, Facile Synthesis of Few-Layer Graphene with a Controllable Thickness Using Rapid Thermal Annealing, Acs Appl Mater Inter, 4 (2012) 1777-1782.
[29] Y.S. Woo, D.H. Seo, D.-H. Yeon, J. Heo, H.-J. Chung, A. Benayad, J.-G. Chung, H. Han, H.-S. Lee, S. Seo, J.-Y. Choi, Low temperature growth of complete monolayer graphene films on Ni-doped copper and gold catalysts by a self-limiting surface reaction, Carbon, 64 (2013) 315-323.
[30] in, Gwyddion version 2.36 (Czech Metrology Institute).
[31] M.S. Dresselhaus, A. Jorio, A.G. Souza, R. Saito, Defect characterization in graphene and carbon nanotubes using Raman spectroscopy, Philos T R Soc A, 368 (2010) 5355-5377.
[32] A.C. Ferrari, Raman spectroscopy of graphene and graphite: Disorder, electron-phonon coupling, doping and nonadiabatic effects, Solid State Commun, 143 (2007) 47-57.
[33] J.B. Wu, X. Zhang, M. Ijas, W.P. Han, X.F. Qiao, X.L. Li, D.S. Jiang, A.C. Ferrari, P.H. Tan, Resonant Raman spectroscopy of twisted multilayer graphene, Nat Commun, 5 (2014) 5309.
[34] K. Kim, S. Coh, L.Z. Tan, W. Regan, J.M. Yuk, E. Chatterjee, M.F. Crommie, M.L. Cohen, S.G. Louie, A. Zettl, Raman spectroscopy study of rotated double-layer graphene: misorientation-angle dependence of electronic structure, Phys Rev Lett, 108 (2012) 246103.
[35] B. Subramanian, S. Jayakumar, M. Jayachandran, S. Jayakrishnan, Studies on nickel electrodeposits on dc magnetron sputtered copper substrates, Surf Eng, 21 (2005) 151-155.
[36] G. Anitha, E. Subramanian, Recognition and exposition of intermolecular interaction between CH2H2Cl2 and CHCl3 by conducting polyaniline materials, Sensor Actuat B-Chem, 107 (2005) 605-615.
[37] C.M. Seah, S.P. Chai, A.R. Mohamed, Mechanisms of graphene growth by chemical vapour deposition on transition metals, Carbon, 70 (2014) 1-21.
[38] A. Reina, X.T. Jia, J. Ho, D. Nezich, H.B. Son, V. Bulovic, M.S. Dresselhaus, J. Kong, Large Area, Few-Layer Graphene Films on Arbitrary Substrates by Chemical Vapor Deposition, Nano Lett, 9 (2009) 30-35.
[39] A.L.V. de Parga, F. Calleja, B. Borca, M.C.G. Passeggi, J.J. Hinarejos, F. Guinea, R. Miranda, Periodically rippled graphene: Growth and spatially resolved electronic structure, Phys Rev Lett, 100 (2008) 1-4.
[40] N.R. Gall', E.V. Rut'kov, A.Y. Tontegode, Interaction of silver atoms with iridium and with a two-dimensional graphite film on iridium: Adsorption, desorption, and dissolution, Phys Solid State+, 46 (2004) 371-377.
[41] S. Marchini, S. Gunther, J. Wintterlin, Scanning tunneling microscopy of graphene on Ru(0001), Phys Rev B, 76 (2007) 1-9.
[42] A.G. Starodubov, M.A. Medvetskii, A.M. Shikin, V.K. Adamchuk, Intercalation of silver atoms under a graphite monolayer on Ni(111), Phys Solid State+, 46 (2004) 1340-1348.

[43] D.E. Starr, E.M. Pazhetnov, A.I. Stadnichenko, A.I. Boronin, S.K. Shaikhutdinov, Carbon films grown on Pt(111) as supports for model gold catalysts, Surf Sci, 600 (2006) 2688-2695.
[44] H. Ueta, M. Saida, C. Nakai, Y. Yamada, M. Sasaki, S. Yamamoto, Highly oriented monolayer graphite formation on Pt(111) by a supersonic methane beam, Surf Sci, 560 (2004) 183-190.
[45] J. Vaari, J. Lahtinen, P. Hautojarvi, The adsorption and decomposition of acetylene on clean and K-covered Co(0001), Catal Lett, 44 (1997) 43-49.
[46] A. Dahal, M. Batzill, Graphene-nickel interfaces: a review, Nanoscale, 6 (2014) 2548-2562.
[47] L. Baraton, Z.B. He, C.S. Lee, C.S. Cojocaru, M. Chatelet, J.L. Maurice, Y.H. Lee, D. Pribat, On the mechanisms of precipitation of graphene on nickel thin films, Epl-Europhys Lett, 96 (2011) 1-6.